

RSC Advances



This is an *Accepted Manuscript*, which has been through the Royal Society of Chemistry peer review process and has been accepted for publication.

Accepted Manuscripts are published online shortly after acceptance, before technical editing, formatting and proof reading. Using this free service, authors can make their results available to the community, in citable form, before we publish the edited article. This *Accepted Manuscript* will be replaced by the edited, formatted and paginated article as soon as this is available.

You can find more information about *Accepted Manuscripts* in the [Information for Authors](#).

Please note that technical editing may introduce minor changes to the text and/or graphics, which may alter content. The journal's standard [Terms & Conditions](#) and the [Ethical guidelines](#) still apply. In no event shall the Royal Society of Chemistry be held responsible for any errors or omissions in this *Accepted Manuscript* or any consequences arising from the use of any information it contains.

Ab initio study on optical properties of glycine sodium nitrate: A novel semiorganic nonlinear optical crystal

M. Dadsetani^{*}, A.R. Omid[†]

Physics Department, Lorestan University, Khorramabad, Iran

Abstract

The electronic structure, linear and nonlinear optical susceptibilities of crystalline glycine-sodium nitrate (GSN) has been studied using the full potential linear augmented plane wave method within density-functional theory. In addition, we have investigated the excitonic effects by means of the bootstrap exchange-correlation kernel within time dependent density functional theory. The crystal in question has band structure with low dispersion which is a characteristic behavior of molecular crystals. Findings show that the inorganic nitrate group play major role in enhancing the optical response of this semi-organic crystal. Although, GSN shows smaller nonlinear response, in comparison with organic crystals, but it has wide range of transparency as well as sufficient anisotropy, which make it promising crystal for nonlinear applications. This study show that $\chi_{yx}^{(2)}$ is more important in infrared region of spectra, while $\chi_{zy}^{(2)}$ possesses the dominant peak in ultraviolet region. In addition to the high potential of excitonic effects, the investigated crystal shows extremely small wavelengths of plasmon peaks.

Keywords:

Semi-organic compound, Ab initio calculations, Electronic structure, Optical properties

^{*} *Corresponding author: Mehrdad Dadsetani*

Email: dadsetani.m@lu.ac.ir

Tel/fax: +98-66-33120192

[†] *Email: omidi_alireza@yahoo.com*

1. Introduction

Since the invention of the laser in 1960, there have been significant developments in the field of nonlinear optical materials. Among the nonlinear optical (NLO) materials, organic materials have attracted a great deal of attention, as they have large optical susceptibilities, inherent ultrafast response time and high optical threshold for laser power compared with inorganic materials [1]. During the last decades, extensive studies have been devoted to achieving a better understanding of factors that may lead to acentric crystals with large NLO responses. Recent studies have shown that semi-organic materials, especially from the amino acid family, are promising candidates for NLO applications as they tend to combine the features of organic with that of inorganic materials [2]. They have several attractive properties such as high NLO coefficient, high damage threshold, wide transparency range, high mechanical strength and thermal stability. The amino acids have interesting physical and chemical properties, since they have chiral symmetry as well as the electron acceptor carboxyl acid ($-\text{COOH}$) group and the electron donor amino ($-\text{NH}_2$) group. Combinations of amino acids with other organic and inorganic materials, give rise to prominent NLO materials, such as l-arginine phosphate, l-arginine hydrochloride, l-histidine tetrafluoroborate, l-alanine tetrafluoroborate, l-histidine bromide, etc. Glycine is the simplest amino acid which has a basic role in the structure of Glycine-sodium nitrate (GSN), as a new NLO crystal. The crystalline GSN ($\text{C}_2\text{H}_5\text{N}_2\text{NaO}_5$) has proven to be a suitable candidate for NLO applications, and the SHG efficiency of this crystal was found to be greater than that of potassium dihydrogen phosphate (KDP) crystal [3]. The crystal band structure, the density of states and the optical absorption of GSN were studied both theoretically and experimentally [4]. Vijayakumaret al. [5] have reported the vibrational spectral analysis of this material using FT-Raman and FT-IR spectroscopy. It is found that GSN is thermally stable up to $198\text{ }^\circ\text{C}$ [6]. Suresh et al. [7] have reported the density measurements, the dielectric studies and the dependence of extinction coefficient (k) and refractive index (n) on the absorption of GSN. In addition, the thermal analyses, the dielectric behavior, the mechanical strength and the work hardening co-efficient of GSN were studied by J. Mary Linet and S. Jerome Das, experimentally [8]. Also, there are studies about the effect of PH on crystal growth [9] and SHG [10] of GSN.

This study tries to give new information about the linear and nonlinear optical properties of GSN within the framework of DFT theory. To the best of our knowledge, there are no ab initio full band structure reports on the nonlinear optical response of GSN. In addition, the mBJ-based calculations for the linear optical response and the electronic structure have been reported for the first time. It's worth mentioning that, in the most of theoretical simulations for nonlinear optic, the bulk susceptibilities are calculated from a straightforward tensor sum over the microscopic (molecular) properties [11,12], while a more comprehensive approach is the

full treatment of periodic crystals by means of band structure theory, although a few studies have used ab-initio full band-structure model to calculate the linear and nonlinear optical responses of crystals. Also, this study tries to investigate the excitonic effects of GSN crystal using Time Dependent Density Functional Theory (TDDFT) [13,14]. Such a study (on GSN crystal) has not been reported earlier. We have used Bootstrap approximation which is known to give optical spectra in excellent agreement with experiments [15], and is computationally less expensive than solving the Bethe Salpeter equation. The differences between TDDFT and RPA results show clear signatures of excitonic effects.

Since the nonlinear susceptibilities are very sensitive to the energy gap, we have used mBJ [16] approximation which can efficiently improve the band gap and give better band splitting. Studies have shown that the mBJ potential is generally as accurate in predicting the energy gaps of many semiconductors as the much more expensive GW method [17].

Next section presents the basic theoretical aspects and computational details of our study. The calculated electronic structure and the optical response are presented in section 3. Last section is devoted to the summary and principle conclusions.

2. Computational details

A. Calculation parameters

Our calculations were performed using the highly accurate all-electron full potential linearized augmented plane wave (FP-LAPW) method based on DFT as implemented in the ELK code [18]. This is an implementation of the DFT with different possible approximation for the exchange correlation (XC) potentials. We have used the *generalized gradient approximation (GGA) of Perdew-Burke-Ernzerhoft* [19] and the modified Becke-Johnson exchange potential (mBJ) [16,17], for the exchange-correlation potentials. The mBJ exchange potential is available through an interface to the Libxc library [20]. Basis functions are expanded in combinations of spherical harmonic functions inside non-overlapping spheres at the atomic sites (muffin-tin spheres) and in plane waves in the interstitial regions. The muffin-tin radii for Oxygen (O), Nitrogen (N), Sodium (Na), hydrogen (H) and carbon (C) was taken to be 1.16, 1.16, 2.2, 0.6 and 1.18 a.u., respectively. The interstitial plane wave vector cut off K_{max} is chosen such that $R_{MT}K_{max}$ equals 5 for all the calculations. The convergence parameter $R_{mt}K_{max}$, where K_{max} is the plane-wave cut-off and R_{mt} is the smallest of all atomic sphere radii, controls the size of the basis. The valence wave functions inside the spheres are expanded up to $l_{max}=10$ while the charge density was Fourier expanded up to $G_{max}=14$. We found the optical spectra to be sufficiently well converged with 300 k-points in the IBZ, and self-consistency was achieved by an iterative process with energy convergence up to 0.0001 eV.

We have used the FHI-aims code [21] for relaxing the atomic positions and structural parameters. FHI-aims uses numeric atom-centered orbitals as the quantum-mechanical basis set:

$$\varphi_i(r) = \frac{u_i(r)}{r} Y_{lm}(\theta, \varphi) \quad (1)$$

Where, $Y_{lm}(\theta, \varphi)$ are spherical harmonics and the radial $u_i(r)$ parts are numerically tabulated. Hence, the bases are very flexible and any kind of desired shape can be achieved. This enables accurate all-electron full-potential calculations at a computational cost which is competitive with plane wave methods. It should be noted that, FHI-aims is an efficient computer program package to calculate physical and chemical properties of condensed matter and other cases, such as molecules, clusters, solids, liquids. We have relaxed the structures (including Van der Waals corrections) in a way that every component of the forces acting on the atoms was less than $10^{-4} eV/\text{\AA}$.

B. Mathematical framework of optical response

We have calculated both linear and non-linear optical spectroscopy within independent particle picture. In addition, sophisticated calculation of linear optical spectra by solving linear response time-dependent density functional theory (TDDFT) equation using bootstrap exchange-correlation kernel is presented. The linear optical properties of matter can be described by means of the transverse dielectric function $\varepsilon(\omega)$. There are two contributions to $\varepsilon(\omega)$, namely, intra-band and inter-band transitions. We ignored the intra-band contribution, since it is important only for metals. The components of dielectric function were calculated using the traditional expression in the random phase approximation (RPA) [22-24]:

$$\varepsilon^{ij}(\omega) = \delta^{ij} + \frac{4\pi i}{\omega} \left[-\frac{i}{\Omega} \sum_k W_k \sum_{cv} \frac{1}{\varepsilon_{vc}} \left(\frac{p_{vc}^i(k) p_{cv}^j(k)}{(\omega + \varepsilon_{vc} + i\eta)} + \frac{(p_{vc}^i(k) p_{cv}^j(k))^*}{(\omega - \varepsilon_{vc} + i\eta)} \right) \right]$$

(2)

Where the term in the bracket is optical conductivity (atomic units are used in the above formula). The sum covers all possible transitions from the occupied to unoccupied states. The term p_{cv}^j denotes the momentum matrix element transition from the energy level c of the conduction band to the level v of the valence band at certain k -point in the BZ . $\hbar\omega$ is the energy of the incident photon and $\varepsilon_{vc} \equiv \varepsilon_v - \varepsilon_c$ is the differences between valence and conduction eigenvalue. W_k is the weight of k -points over the Brillouin zone and Ω is the unit cell volume.

Time-dependent density-functional theory (TDDFT) [25], which extends density-functional theory into the time domain, is another method which is able, in principle, to determine neutral excitations of a system. The TDDFT method can handle large systems and is, basically, exact. Hence, this study tries to cover both the RPA- and TDDFT-based linear optical responses. The key quantity of TDDFT is the exchange-correlation kernel f_{xc} , which, together with the Kohn-Sham (KS) single-particle density-response function χ^s , determines the interacting-particles density-response function χ , as follows:

$$\chi_{GG'}^{-1}(q, \omega) = (\chi^s)_{GG'}^{-1}(q, \omega) - \frac{4\pi}{|G+q|^2} \delta_{GG'} - f_{GG'}^{xc}(q, \omega) \quad (3)$$

While χ^s is constructed using the single-particle states obtained with a given approximation to the static exchange-correlation potential $V_{xc}(r)$ [26], f_{xc} is a true many-body quantity, basically, containing all the dynamic exchange-correlation effects in a real interacting system. Although formally exact, the predictions of TDDFT are only as good as the approximation of the exchange-correlation kernel. A great amount of effort has been invested into the development of approximations to f_{xc} of semiconductors and insulators [27-35]. In

this study, we have used the Bootstrap approximation for f_{xc} [15] which has a wide applicability and is computationally less expensive than solving the Bethe Salpeter equation. The exact relationship between the dielectric function and the kernel f_{xc} for a periodic solid can be written as:

$$\begin{aligned}\varepsilon_{GG'}^{-1}(q, \omega) &= \delta_{GG'} + v_{GG'}(q)\chi_{GG'}(q, \omega) \\ &= \delta_{GG'} + \chi_{GG'}^s(q, \omega)v_{GG'}(q)\{(1 - [v_{GG'}(q) + f_{GG'}^{xc}(q, \omega)]\chi_{GG'}^s(q, \omega)\}^{-1}\end{aligned}\quad (4)$$

Here $v(q)$ is the bare Coulomb potential. All these quantities are matrices on the basis of reciprocal lattice vectors G . The Bootstrap exchange-correlation is approximated by

$$f_{xc}^{boot}(q, \omega) = -\frac{\varepsilon^{-1}(q, \omega=0)v(q)}{\varepsilon_0^{00}(q, \omega=0) - 1} = \frac{\varepsilon^{-1}(q, \omega=0)}{\chi_0^{00}(q, \omega=0)}\quad (5)$$

Where $\varepsilon_0(q, \omega) = 1 - v(q)\chi(q, \omega)$ denotes the dielectric function in RPA. The superscript 00 indicates that only the $G=G'=0$ component is used in the denominator. This coupled set of equations is solved by first setting $f_{xc}^{boot} = 0$ and then solving (4) to obtain ε^{-1} . This is then ‘‘bootstrapped’’ in (5) to find a new f_{xc}^{boot} , and the procedure is repeated until self-consistency between the two equations at $\omega=0$ is achieved.

In addition to the linear response, this study tries to cover the nonlinear response of investigated crystals. The mathematical relations for calculating the second order susceptibilities as well as their inter- and intra-band contributions have been developed by Sipe and Ghahramani [36], and Aversa and Sipe [37]. Within the independent particle picture, the complex second-order nonlinear optical susceptibility tensors can be written as [38-44]:

$$\chi_{ijk}^{inter}(-2\omega, \omega, \omega) = \frac{1}{\Omega} \sum_{nmlk} W_k \left\{ \frac{2r_{nm}^i \{ \vec{r}_{ml}^j \vec{r}_{ln}^k \}}{(\omega_{ln} - \omega_{ml})(\omega_{mn} - 2\omega)} - \frac{1}{(\omega_{mn} - \omega)} \left[\frac{\vec{r}_{lm}^k \{ \vec{r}_{mn}^i \vec{r}_{nl}^j \}}{(\omega_{nl} - \omega_{mn})} - \frac{\vec{r}_{nl}^j \{ \vec{r}_{lm}^k \vec{r}_{mn}^i \}}{(\omega_{lm} - \omega_{mn})} \right] \right\} \quad (6)$$

$$\begin{aligned}\chi_{ijk}^{intra}(-2\omega, \omega, \omega) &= \frac{1}{\Omega} \sum_k W_k \left\{ \sum_{nml} \frac{\omega_{mn}^{-2}}{(\omega_{mn} - \omega)} [\omega_{ln} \vec{r}_{nl}^j \{ \vec{r}_{lm}^k \vec{r}_{mn}^i \} - \omega_{ml} \vec{r}_{lm}^k \{ \vec{r}_{mn}^i \vec{r}_{nl}^j \}] \right. \\ &\quad \left. - 8i \sum_{nm} \frac{\vec{r}_{nm}^i \{ \Delta_{mn}^j \vec{r}_{nm}^k \}}{\omega_{mn}^2 (\omega_{mn} - 2\omega)} + 2 \sum_{nml} \frac{\vec{r}_{nm}^i \{ \vec{r}_{ml}^j \vec{r}_{ln}^k \} (\omega_{ml} - \omega_{ln})}{\omega_{mn}^2 (\omega_{mn} - 2\omega)} \right\}\end{aligned}\quad (7)$$

$$\chi_{ijk}^{mod}(-2\omega, \omega, \omega) = \frac{1}{2\Omega} \sum_k W_k \left\{ \sum_{nml} \frac{1}{\omega_{mn}^2 (\omega_{mn} - \omega)} [\omega_{nl} \vec{r}_{lm}^i \{ \vec{r}_{mn}^j \vec{r}_{nl}^k \} - \omega_{lm} \vec{r}_{nl}^i \{ \vec{r}_{lm}^j \vec{r}_{mn}^k \}] - i \sum_{nm} \frac{\vec{r}_{nm}^i \{ \vec{r}_{nm}^j \Delta_{mn}^k \}}{\omega_{mn}^2 (\omega_{mn} - \omega)} \right\} \quad (8)$$

From these formulae (atomic units are used in these relations), we can notice that there are three major contributions to $\chi_{ijk}^{(2)}(-2\omega, \omega, \omega)$: the inter-band transitions $\chi_{ijk}^{inter}(-2\omega, \omega, \omega)$, the intra-band transitions

$\chi_{ijk}^{\text{int } ra}(-2\omega, \omega, \omega)$, and the modulation of inter-band terms by intra-band terms $\chi_{ijk}^{\text{mod}}(-2\omega, \omega, \omega)$, where $n \neq m \neq l$ and i, j and k correspond to Cartesian indices.

Here, n denotes the valence states, m denotes the conduction states, and l denotes all states ($l \neq m, n$). Two kinds of transitions take place: one of them is vcc' which involves one valence band (v) and two conduction bands (c and c') and the second transition is $vv'c$ which involves two valence bands (v and v') and one conduction band (c). The symbols $\Delta_{nm}^i(\vec{k})$ and $\{r_{nm}^i(\vec{k})r_{ml}^j(\vec{k})\}$ are defined as follows:

$$\Delta_{nm}^i(\vec{k}) = v_{nm}^i(\vec{k}) - v_{mm}^i(\vec{k}) \quad (9)$$

$$\{r_{nm}^i(\vec{k})r_{ml}^j(\vec{k})\} = \frac{1}{2}(r_{nm}^i(\vec{k})r_{ml}^j(\vec{k}) + r_{nm}^j(\vec{k})r_{ml}^i(\vec{k})) \quad (10)$$

Where \vec{v}_{nm}^i is the i component of the electron velocity (given as $\vec{v}_{nm}^i(k) = i\omega_{nm}(k)r_{nm}^i(\vec{k})$). The position matrix elements between band states n and m , $r_{nm}^i(\vec{k})$, are calculated from the momentum matrix element \vec{p}_{nm}^i using

the relation [45]: $r_{nm}^i(\vec{k}) = \frac{p_{nm}^i(\vec{k})}{im\omega_{nm}(\vec{k})}$, where the energy difference between the states n and m are given by

$\hbar\omega_{nm} = \hbar(\omega_n - \omega_m)$ and W_k is the weight of k -points.

As mentioned before, GSN is a non-centrosymmetric crystal which has eight second order nonlinear susceptibilities: $xyx, yxy, yzy, zxx, zxz, zyy, zzx$ and zzz . According to the results of this study, $\chi_{zyy}^{(2)}$ possesses the dominant peaks of nonlinear response.

3. RESULTS AND DISCUSSION

A. Crystal structure, electronic and linear optical properties

Fig. 1 shows the unit cell as well as different views of GSN crystal structure. The asymmetric unit of GSN consists of one glycine molecule, one sodium cation and one nitrate anion. As can be seen in Fig. 1A, the glycine molecules are located between layers of $NaNO_3$ chains and linked to sodium nitrate by strong intramolecular hydrogen bonds of N-H—O type. The zwitterion forms of glycine provide an antiparallel arrangement and non-centrosymmetric crystalline growth. Although the polarity of glycine molecules changes alternately, they cannot nullify each other completely. In addition, the crystal seems as infinite chains in the ac plane. The NLO activity of crystal can be attributed to the structural organization of infinite chains of highly polarity entities connected in a head to tail arrangement in GSN. Experimental studies have shown that GSN has a monoclinic non-centrosymmetric crystalline structure with space group Cc . The optimized lattice parameters for crystalline GSN ($a=14.329$ Å, $b=5.2662$ Å, $c=9.1129$ Å, $\alpha=\gamma=90^\circ$ and $\beta=119.10^\circ$) are found to be in good agreement with the X-ray crystallographic data [46,47]. The crystallographic a and b axes are parallel to the optical x and y axes, respectively, but the c-axis deviates from the z-axis by about 29° . The polarization axis of glycine molecule is very close to the y-axis; in addition, the molecular plane of nitrate group is mainly located in the b-c plane, hence ϵ_{yy} exhibits the maximum values of dielectric function. On the other hand, the planes containing glycine and nitrate groups are mainly perpendicular to the x-axis giving the smallest values of ϵ_{xx} , since there is very little electronic response out of the molecular plane.

In table 1, we have presented the respective geometrical parameters such as bond lengths and bond angles of optimized structure. In spite of small deviations, the optimized values of bond angles and bond lengths are very close to the experimental values. For example, the calculated C-H and N-H bonds are slightly longer than their experimental counterparts. Due to the strong N-H—O hydrogen bonding of NH_3 group, with the oxygen of the carbonyl group, the optimization procedure (including Van der Waals correction) gives smaller values for the bond angle $C_9-N_{12}-H_{14}$. On the other hand, the attraction between nitrate group (NO_3) and sodium (Na) atom makes the bond angle $Na_5-O_6-C_7$ smaller than experimental value. It should be noted that, the nitrate group has planar form in both experimental and optimized regimes.

In what follows, the electronic band structure, and total and partial densities of electron states are presented. Fig. 2 shows the calculated electronic band structure and the corresponding total DOS, of investigated crystals. As can be seen, the mBJ approximation push the valence bands to lower energies and the conduction bands to higher energies, yielding improved results for the band gap. As a result of low intermolecular

interactions, both GGA and mBJ approximation give band structures with low dispersions. Moreover, when we go from GGA to mBJ, an empty region with no energy bands appears in the range of 4-6 eV. In the rest of this study, we will report our results using mBJ only, since it gives better band gap and better band splitting. The results of our calculations using mBJ (GGA) approximation gives a fundamental direct band gap value of 5.32 eV (3.38 eV) at Γ , while J. Herná'ndez-Paredes and colleagues [4] have reported the band gap value of 2.98 (2.99) eV with LDA (GGA) approximation, which is smaller than our result. Suresh et al. have evaluated the band gap by the extrapolation of the linear part of optical absorption (α) spectrum [7]. They found the band gap to be 4.0 eV, which is smaller than the calculated value with mBJ approximation. In other experimental study [8], one can see a sharp decrease (at around $\lambda=240\text{nm}$) in absorption spectra of GSN crystal which shows good agreement with calculated band gap within mBJ approximation.

In sum, the GSN crystal has a wide range of transparency which is desirable for NLO applications, since the absorptions near the fundamental or second harmonic signals will lead to the loss of the conversion of SHG.

In order to show the role that different groups play, we have reported the partial density of states for functional groups, separately. As can be seen in Fig. 3, the the p-states of NO_3 play major roles in the top of valence bands and the bottom of conduction bands. According to this figure, the inorganic nitrate group has important role in the optical activity of GSN crystal, since the main peaks of optical response come from electron transitions from the highest valence bands to the lowest group of conduction bands. As expected for molecular crystals, glycine and NO_3 groups create quasi-separated states. It is worth mentioning that, compared to other groups, the sodium atom has negligible contribution to the top valence bands and the bottom of conduction bands. In addition, this figure clearly shows that the glycine and nitrate groups exist as dipolar structures, since they have a sharp electron-donating peak just below the band gap and a sharp electron-withdrawing peak above the band gap. In what follows, the imaginary and real parts of dielectric function and the different components of refractive indices are represented. Assuming that they give a small contribution to the dielectric functions, we ignored the indirect inter-band transitions involving scattering of phonons [48-51]. The Calculated imaginary (ϵ_2^{ii}) and real parts (ϵ_1^{ii}) of dielectric functions are presented in Fig. 4. As can be seen, the imaginary components have two main structures: (i) below 11 eV and (ii) above 11 eV. The dominant peaks are located in part (i), and there is large anisotropy here. All components have a sharp peak (α) around 6.2 eV which (in comparison with Fig. 3) comes from the electron transitions between a-valence bands to the e-conduction bands ($a \rightarrow e$). As mentioned before, the high intensity of $\epsilon_2^{yy}(\omega)$, in part (i), can be attributed to the fact that the polarization vector of glycine molecules are very close to the y-axis; in addition to the molecular planes of nitrate groups which are located in the b-c plane. On the other hand, the

molecular planes of glycine and nitrate groups are mainly perpendicular to the x-axis which makes $\varepsilon_2^{xx}(\omega)$ smallest. The peak β (in $\varepsilon_2^{xx}(\omega)$ and $\varepsilon_2^{zz}(\omega)$) is located around 7.7 eV and comes from the electron transitions between *b*-valence bands to the *f*-conduction bands (*b*→*f*). Both $\varepsilon_2^{xx}(\omega)$ and $\varepsilon_2^{yy}(\omega)$ have another sharp peak (γ) at part (i), which is located around 10.15 eV and come from *d*→*f* transitions. There is a wide hump around 17.5 eV as well as several small peaks at part (ii). The weakness of structures at this part, compared to part (i), can be attributed to the fact that $\varepsilon_2(\omega)$ scales as $1/\omega^2$. Furthermore, the investigated crystal shows large values of $\varepsilon(0)/\varepsilon(\infty)$, whose deviation from one is a sign of the polarity of materials.

The variations of refractive indices of investigated compound are represented in Fig. 5. According to this figures, we can see considerable anisotropy, particularly in non-absorbing region. It should be noted that this anisotropy is necessary for phase-matching conditions. The GSN crystal mainly shows the uniaxial, rather than biaxial, behavior. For example, our calculations give the static values of 1.35, 1.49 and 1.48 for $n_{xx}(0)$, $n_{yy}(0)$ and $n_{zz}(0)$, respectively. We also have represented the variations of refractive indices with wavelength. As can be seen, $n_{xx} < n_{yy} \approx n_{zz}$ and there is sufficient anisotropy for wavelengths above 200nm, which make crystal promising candidate for SHG in IR-VIS and UV- VIS regions. Suresh et. al [7] have measured the refractive index of GSN crystal by Brewster's angle method using He-Ne laser of wavelength 632.8 nm. Their experimental result ($n=1.510$) is very close to our theoretical results ($n_{yy} = 1.5078$ and $n_{zz} = 1.5019$).

B. Nonlinear optical response

In this part of our study, we present our results for the nonlinear optical properties of GSN. It should be mentioned that, the physical interpretation of nonlinear results is very difficult, since in addition to valence-valence and conduction-conduction transitions, both inter- and intra-band transitions can participate in nonlinear procedure. In addition, the nonlinear susceptibilities are very sensitive to slight changes of band dispersion, due to the 2ω and ω resonances which appear in the imaginary and real parts of $\chi^{(2)}$.

The absolute values of nonlinear susceptibilities are represented in Fig. 6. As can be seen, the maximum values of nonlinear response are located around 3 eV and 6.5 eV. The first peak is more important, since it is located below the band gap. Furthermore, $\chi_{yyx}^{(2)}$ and $\chi_{zyy}^{(2)}$ have larger values of nonlinearity at energy values under 1 eV and in the range of 1-2.5 eV, respectively. While, $\chi_{yzy}^{(2)}$ possesses the dominant peak around 3 eV. The imaginary and real parts of $\chi_{yzy}^{(2)}$ as well as $\omega/2\omega$ intra- and inter-band contributions to this element is presented in Fig. 7. According to this figure, the main peak which is located below the band gap, mainly

comes from 2ω intra-band contribution, while both ω intra-band and ω inter-band factors play important role in that sharp peak which is located above the band gap (around 6.5 eV). As can be seen, the 2ω -resonances start to contribute at energies below the band gap ($E \leq E_g/2$), while the ω -contributions come at frequencies above the band gap. This figure also shows opposite symmetrical patterns for the ω - and 2ω -resonances at higher energies which make the high-energy nonlinear response, decrease. Although GSN shows lower values of nonlinear response, in comparison to organic crystals [52], it has sufficient anisotropy and wide range of transparency which make it promising crystal for SHG in IR-VIS and VIS-UV regions. For example, the experimental measurements of GSN [10] have shown that this crystal has a high grade of SHG efficiency at $\lambda=1064\text{nm}$.

In the following, we have presented the linear optical spectra in comparison with nonlinear one, to show the interesting similarities between them. Unlike the linear spectra, the features in the nonlinear spectra are very difficult to identify from the band structure, because of the presence of 2ω and ω resonances. Generally, whenever the inter-band peaks appear, the intra-band peaks appear simultaneously. Since the magnitude of inter-band transitions are realizable from $\varepsilon_2(\omega)$, one could expect the nonlinear structures to be realized from the features of $\varepsilon_2(\omega)$. Hence, we find it useful to compare absolute values of nonlinear susceptibilities with the imaginary parts of dielectric function, as a function of both ω and 2ω (Fig. 8). This figure shows significant similarities between linear and nonlinear spectra. The colored arrows indicate the agreement between nonlinear and linear peak positions (as a function of both ω and 2ω). For example, in the below-band gap region, both linear and nonlinear structures have two peaks (the red and green arrows). The blue arrow shows that both linear and nonlinear regimes have a sharp peak around 6.2 eV. Furthermore, this figure also shows that the below-band gap nonlinear structures originate from the 2ω -resonances, while that nonlinear sharp peak which is located just above the band gap (the blue arrow) mainly comes from the ω -resonances. It can be seen that, the nonlinear structures located in the range of 7-10 eV mainly come from the 2ω -resonances, but the sharp peak around 10 eV, mainly originate from the ω -resonances. Finally, this figure shows that when we move from the linear regime to the nonlinear one, the low-energy peaks are enhanced and shifted to lower energies, but the high-energy peaks tend to be small. As mentioned before, the molecular crystals possess band structure with small dispersions, particularly around the band gap, which enhances the two photon absorption at lower energies. On the other hand, increase in band dispersion at higher energies, makes the two photon absorption diminish. Another reason for this reduction could be explained by the fact that $\chi_2(\omega)$ scales as $1/\omega^2$. Due to valence-valence and conduction-conduction transitions, it is almost

impossible to predict the exact behavior of nonlinear response, although the general behavior can be recognized from the combination of $\epsilon_2(\omega)$ and $\epsilon_2(2\omega)$.

Finally, we can estimate the values of first order hyperpolarizabilities (tensor β_{ijk}) of GSN molecule by using, the expression ($\beta_{ijk} = \chi_{ijk}/Nf^3$) given in Refs. 53 and 54. Here, N is the number of molecules/cm³ and f is the local field factor which its value is varying between 1.3 to 2.0. The calculated value for β_{yyx} of GSN (at $\lambda \approx 1064\text{nm}$) is found to be 2.23×10^{-30} (esu).

C. TDDFT calculations and excitonic effects.

We have used the bootstrap kernel [15] (within the framework of time dependent DFT) to investigate the excitonic effects in GSN crystal. Recent studies show that TDDFT kernels (such as Bootstrap kernel) which have a long range $1/q^2$ contribution in the long-wavelength limit are able to capture the exciton formation in solids [29-34] with low computational cost.

The results of RPA and TDDFT calculations, for the imaginary and real parts of dielectric function of GSN crystal, are represented in Fig. 9. One can see a strong signature of excitonic effects in bulk GSN, by comparing red-shifted TDDFT results with those of RPA. It is clear that, despite the extremely good overall agreement between RPA and TDDFT results, the bootstrap procedure tends to enhance the low-energy structures. In addition, there is a slight red-shift in going from RPA to TDDFT calculations. Although the excitonic effects have minor roles at higher energies, $\epsilon^{(xx)}$ shows considerable deviations at energy values between 10-18 eV.

At the end part of this section, we have shown the electron energy loss spectra of GSN crystal in Fig. 10. The energy loss function, $L(\omega) = \text{Im}[-1/\epsilon]$ is an important factor which illustrates the energy loss of a fast electron traversing in a material. Generally, the energy loss spectra show two main structures. The low-energy peaks (under 10eV) can be attributed to the inter-band transitions between valence and conduction bands. Hence, there is a clear correspondence between the loss peak positions with those of $\text{Im}-\epsilon_{ij}$, but the loss peaks have slight blue-shifts [55]. The second main structure of the loss spectra is a wide peak around 27 eV, which corresponds to the collective plasmon excitations. The plasmon peaks correspond to the abrupt reduction of $\epsilon_2(\omega)$ and to the zero crossing of $\epsilon_1(\omega)$. As can be seen in this figure, the RPA structures are very close to those of TDDFT, but the excitonic effects make the low-energy peaks enhance. In both RPA and TDDFT regimes, L_{xx} has a lower intensity of plasmon peak, while L_{zz} and L_{yy} have close values of intensity.

Like to linear regime, the excitonic effects also can change the optical spectra in nonlinear regime. For example, as shown for the linear optical spectra, the excitonic effects not only can enhance the non-linear optical spectra, especially at lower energies, they can shift the onset of nonlinear response to lower frequencies [56-58].

To sum up, we have used a full ab initio treatment for handling nonlinear response of periodic crystals within the framework of band structure theory. This study gives reliable dispersions for the linear and nonlinear optical spectra in both absorbing and non-absorbing regions. In addition, since the experimental measurement of nonlinear susceptibilities is expensive and somewhat cumbersome, such studies provide an extremely useful guide for research on nonlinear organic crystals. This study provides new valuable information about the optical properties of investigated solid which are a major topic, both in basic research and for industrial applications. According to our study, the investigated crystal has wide range of transparency as well as sufficient anisotropy, in the non-absorbing region, which is important for phase matching. So, GSN crystal can be considered as proper candidate for SHG in the IR-VIS and VIS-UV regions. It should be noted that, our calculations have been conducted based on Van der Waals interactions, which play major roles in the band structure and optical response of molecular crystals.

4. Conclusions

We have studied the electronic structure as well as the linear and nonlinear optical properties of GSN crystal using the FP-LAPW method within the framework of DFT and TDDFT. Our calculations, based on mBJ and GGA approximations, give rise to the direct band gap for this crystal. Regarding the crystal structure, the planes containing nitrate groups and glycine molecules mainly tend to be perpendicular to the x-axis, hence ϵ_{xx} shows the smallest values of dielectric function. This study shows that the inorganic nitrate group plays major role in enhancing the optical response of GSN, since the top of valence bands and the bottom of conduction bands comes from the p-states of nitrate group. In spite of having band structure with low dispersion, due to the high value of band gap, GSN shows smaller nonlinear response, compared to organic crystals. Despite this, it has high thermal stability, sufficient anisotropy and wide range of transparency, which make it promising crystal for SHG. Among the nonlinear optical susceptibilities, $\chi_{yy}^{(2)}$ possesses the dominant peak in non-absorbing region of spectra, while $\chi_{yyx}^{(2)}$ is more important in infrared region. Findings show that the 2ω -resonance intra-band factor plays an important role in the below-band-gap structures of nonlinear spectra. This study shows that there is a significant correspondence between the peak positions of linear spectra (as a function of both ω and 2ω) with those of nonlinear one.

According to the results of our study, the excitonic effects can produce red-shifted enhanced structures, in both linear and nonlinear regimes. Finally, both DFT and TDDFT calculations for the energy loss spectra yield plasmon peaks around 27 eV.

References

- [1] R.A. Hann, D. Bloor, Organic Materials for Nonlinear Optics, *The Royal Society of Chemistry*, 1989, Special publications no. 69.
- [2] R. Sankar, C.M. Ragahvan, R. Mohan Kumar, R. Jayavel, *J. Cryst. Growth*, 309 (2007) 30.
- [3] M. Narayan Bhat, S.M. Dharmaprakash, *J. Cryst. Growth*, 235 (2001) 511.
- [4] J. Hernandez-Paredes, D. Glossman-Mitnik, H.E. Esparza-Ponce, M.E. Alvarez-Ramos, A. Duarte-Moller, *J. Mol. Struct.* 875 (2008) 295.
- [5] T. Vijayakumar, I. Hubert Joe, C.P. Reghunadhan Nair, V.S. Jayakumar, *J. Mol. Struct.* 877 (2008) 20.
- [6] J. Hernandez-Paredes, O. Daniel Glossman-Mitnik, H. Hernandez-Negrete, M.E. Esparza-Ponce, R. Alvarez, R. Rodriguez Mijangos, A. Duarte-Moller, *J. Phys. Chem. Solids* 69 (2008) 1974.
- [7] S. Suresh, A. Ramanand, P. Mani, *Journal of Optoelectronics and Biomedical Materials*, 1 (2010) 129.
- [8] J. Mary Linet and S. Jerome Das, *Optik* 123 (2012) 1895.
- [9] S. Palaniswamy and O.N. Balasundaram, *Rasayan j. chem.* 2 (2009) 386.
- [10] R. A. Silva-Molina *et al.* *Natural Science* 3 (2011) 319-322.
- [11] D.S. Chemla, J.L. Oudar, J. Jerphagnon, *Phys. Rev. B* 12 (1975) 4534.
- [12] J. Zyss, J.L. Oudar, *Phys. Rev. A* 26 (1982) 2028.
- [13] E. Runge and E.K.U. Gross, *Phys. Rev. Lett.* **52** (1984) 997.
- [14] E.K.U. Gross, F.J. Dobson and M. Petersilka, *Density Functional Theory*, Springer, New York, (1996).
- [15] S. Sharma, J. K. Dewhurst, A. Sanna, and E. K. U. Gross, *Phys. Rev. Lett.* 107 (2011) 186401
- [16] F. Tran and P. Blaha, *Phys. Rev. Lett.* 102 (2009) 226401.
- [17] D. Koller, F. Tran and P. Blaha, *Phys. Rev. B* 83 (2011) 195134.
- [18] Elk FP-LAPW code, K. Dewhurst, S. Sharma, L. Nordstrom, F. Cricchio, F. Bultmark, H. Gross, C. Ambrosch-Draxl, C. Persson, C. Brouder, R. Armiento, et al. (<http://elk.sourceforge.net/>).
- [19] J. P. Perdew, K. Burke and M. Ernzerhof, *Phys. Rev. Lett.* 77 (1997) 3865.
- [20] M. A. L. Marques, M. J. T. Oliveira and T. Burnus, *Comput. Phys. Commun.* 183 (2012) 2272.
- [21] V. Blum, R. Gehrke, F. Hanke, P. Havu, V. Havu, X. Ren, K. Reuter, M. Scheffler, *Computer Physics Communications* 180 (2009) 2175.
- [22] G. Grosso and G. P. Parravicini, *Solid state physics*, Academic Press, San Diego, (2000).
- [23] F. Bassani and G. P. Parravicini, *Electronic States and Optical Transitions in Solids*, Pergamon, Oxford, 1975, pp. 149–154.
- [24] H. Rathgen and M. I. Katsnelson, *Physica Scripta*. 109 (2004) 170.
- [25] E. K. U. Gross and W. Kohn, *Phys. Rev. Lett.* 55 (1985) 2850.
- [26] W. Kohn and L. J. Sham, *Phys. Rev. A*. 140 (1965) 1133.
- [27] Y. H. Kim and A. G̃orling, *Phys. Rev. B*. 66 (2002) 035114.
- [28] Y. H. Kim and A. G̃orling, *Phys. Rev. Lett.* 89 (2002) 096402.
- [29] F. Sottile, V. Olevano, and L. Reining, *Phys. Rev. Lett.* 91(2003) 056402.
- [30] S. Botti, F. Sottile, N. Vast, V. Olevano, L. Reining, H. C. Weissker, A. Rubio, G. Onida, R. Del Sole, and R.W. Godby, *Phys. Rev. B* 69 (2004) 155112.
- [31] V. U. Nazarov and G. Vignale, *Phys. Rev. Lett.* 107 (2011) 216402.
- [32] Z. H. Yang, Y. Li, and C. A. Ullrich, *The Journal of Chemical Physics*, 137 (2012) 014513.
- [33] J. E. Bates and F. Furche, *The Journal of Chemical Physics*, 137 (2012) 164105.
- [34] Z. H. Yang and C. A. Ullrich, *Phys. Rev. B*. 87 (2013) 195204.
- [35] P. E. Trevisanutto, A. Terentjevs, L. A. Constantin, V. Olevano, and F. D. Sala, *Phys. Rev. B*. 87 (2013) 205143.

- [36] J.E. Sipe and E. Ghahramani, *Phys. Rev. B.* 48 (1993) 11705.
- [37] C. Aversa and J.E. Sipe, *Phys. Rev. B.* 52 (1995) 14636.
- [38] S. Sharma, J. K. Dewhurst and C. Ambrosch-Draxl, *Phys. Rev. B.* 67 (2003) 165332.
- [39] S. Sharma and C. Ambrosch-Draxl, *PhysicaScripta T.* 109 (2004) 128.
- [40] A. H. Reshak, Ph.D. thesis, Indian Institute of Technology-Rooke, India, (2005).
- [41] A. H. Reshak, *J. Chem. Phys.* 125 (2006) 014708.
- [42] A. H. Reshak, *J. Chem. Phys.* 124 (2006) 014707.
- [43] S. N. Rashkeev and W. R. L. Lambrecht, *Phys. Rev. B.* 63 (2001) 165212.
- [44] S. N. Rashkeev, W. R. L. Lambrecht, and B. Segall, *ibid.* 57 (1998) 3905.
- [45] C. Ambrosch-Draxl and J. Sofo, *Comput. Phys. Commun.* 175 (2006) 1.
- [46] R.V. Krishnakumar, M. Subha Nandhini, S. Natarajan, K. Sivakumar, Babu Varghese, *Acta Crystallagr. C57* (2001) 1149.
- [47] M. Narayan Bhat, S.M. Dharmaparakash, *J. Cryst. Growth* 235 (2002) 511–516.
- [48] A. H. Reshak, D. Stys, S. Auluck, *J. Phys. Chem. B*, 114 (2010) 1815..
- [49] A. H. Reshak, S. Auluck, D. Stys, I. V. Kityk, H. Kamarudin, J. Berdowski, Z. Tylczynski, *J. Mater. Chem.* 21(2011) 17219.
- [50] A. H. Reshak, H. Kamarudin, I. V. Kityk, S. Auluck, *J. Phys. Chem. B* 116 (2012) 13338.
- [51] A. H. Reshak, D. Stys, S. Auluck, I. V. Kityk, *J. Phys. Chem. B* 113 (2009) 12648.
- [52] M. Dadsetani, A. R. Omid, *J. Phys. Chem. Solids*, 85 (2015) 117.
- [53] R. W. Boyd, *Nonlinear Optics, Academic Press, 3rd edn*, 2008.
- [54] T. Seidler, K. Stadnicka, B. Champagne, *J. Chem. Phys.* 141 (2014) 104109.
- [55] A. Alkauskas, S. D. Schneider, S. Sagmeister, C. Ambrosch-Draxl, C. Hébert, *Ultramicroscopy*, 110 (2010) 1081.
- [56] R. Leitsmann, W. G. Schmidt, P. H. Hahn and F. Bechstedt, *Phys. Rev. B* 71 (2005) 195209.
- [57] M. Grüning and C. Attaccalite, *Phys. Rev. B* 90 (2014) 199901.
- [58] E. Luppi, H. Hübener and V. Véniard, *Phys. Rev. B* 82 (2010) 235201.

Appendix:

<i>symbol</i>	<i>Definition</i>
<i>GSN</i>	<i>Glycine-sodium nitrate</i>
<i>DFT</i>	<i>Density functional theory</i>
<i>TDDFT</i>	<i>Time dependent density functional theory</i>
<i>NLO</i>	<i>Nonlinear optic</i>
<i>GGA</i>	<i>Generalized gradient approximation</i>
<i>mBJ</i>	<i>Modified Becke-Johnson exchange potential</i>
<i>RPA</i>	<i>Random Phase Approximation</i>
<i>KS</i>	<i>Kohn-Sham</i>
ϵ_2^{ii}	<i>Imaginary parts of dielectric function</i>
ϵ_1^{ii}	<i>Real parts of dielectric function</i>
n_{ii}	<i>The i-component of refractive index</i>
L_{ii}	<i>The i-component of energy loss function</i>
P_{nm}^j	<i>Momentum matrix elements</i>
W_k	<i>Weight of k-points over the Brillouin zone</i>
Ω	<i>The unit cell volume</i>
f_{xc}	<i>Exchange-correlation kernel</i>
$V_{xc}(\mathbf{r})$	<i>Exchange-correlation potential</i>
$f_{xc}^{boot}(q, \omega)$	<i>Bootstrap exchange-correlation kernel</i>
$\chi_{ijk}^{(2)}(-2\omega, \omega, \omega)$	<i>Second-order nonlinear optical susceptibilities</i>
$\chi_{ijk}^{inter}(-2\omega, \omega, \omega)$	<i>Inter-band contribution to nonlinear susceptibilities</i>
$\chi_{ijk}^{intra}(-2\omega, \omega, \omega)$	<i>Intra-band contribution to nonlinear susceptibilities</i>
$\chi_{ijk}^{mod}(-2\omega, \omega, \omega)$	<i>Modulation of inter-band terms by intra-band terms in nonlinear procedure</i>
β_{ijk}	<i>First order hyperpolarizabilities</i>
$r_{nm}^i(\vec{k})$	<i>Position matrix elements between band states n and m</i>
\vec{v}_{nm}^i	<i>The i component of the electron velocity</i>
$\Delta_{nm}^i(\vec{k})$	<i>The difference between electron-velocities of states n and m</i>

$\hbar\omega_{nm}$	<i>The energy difference between the states n and m</i>
--------------------	---

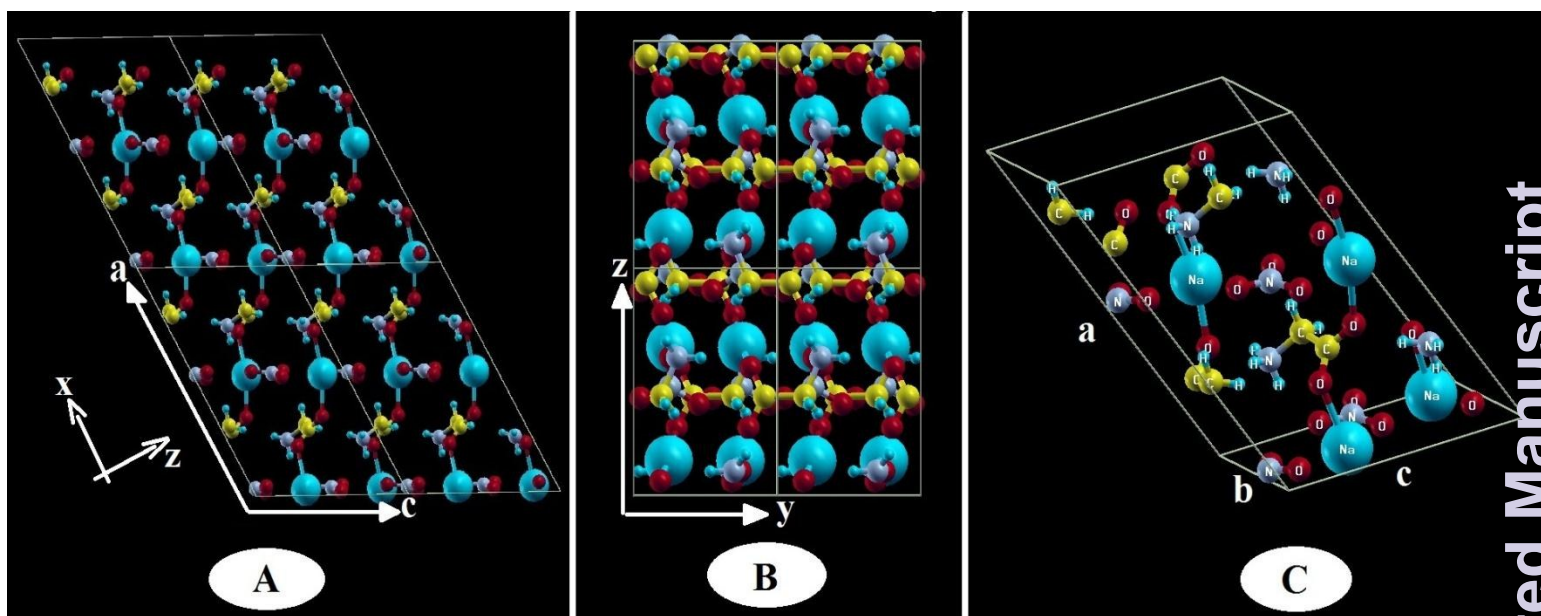


Fig. 1. The crystal structure along y-axis (A), the crystal structure along x-axis (B), the unit-cell of crystal (C).

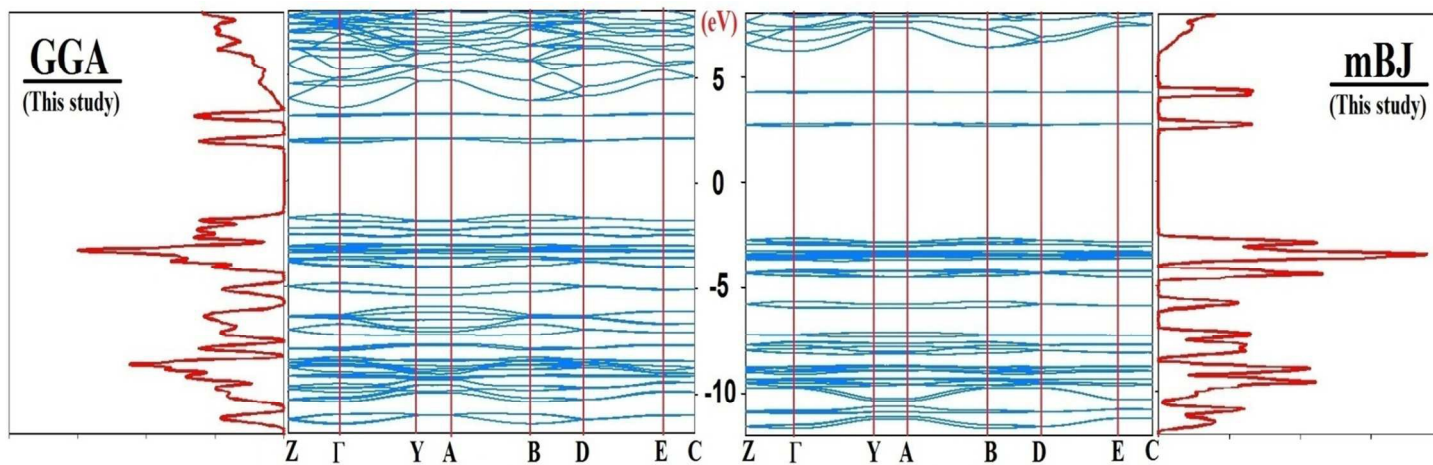


Fig. 2. Our results for the band structure and total DOS of GSN crystal using m-BJ and GGA approximations.

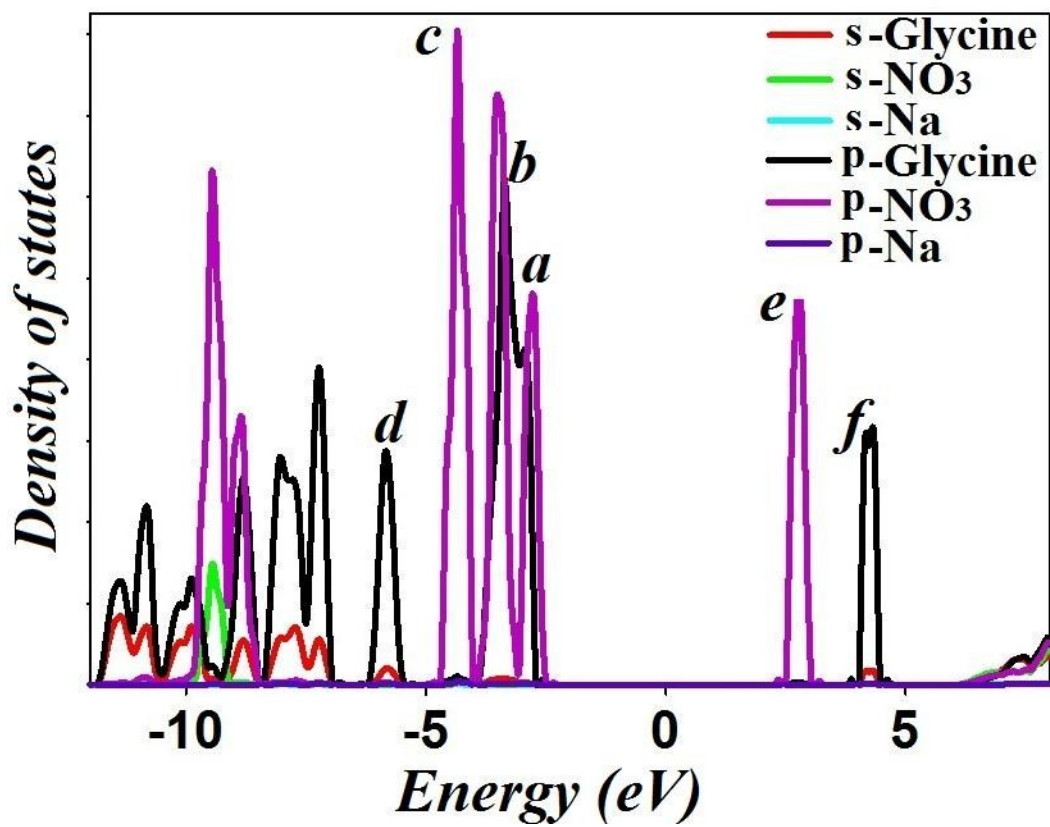


Fig. 3. Calculated density of states for the different functional groups of GSN crystal.

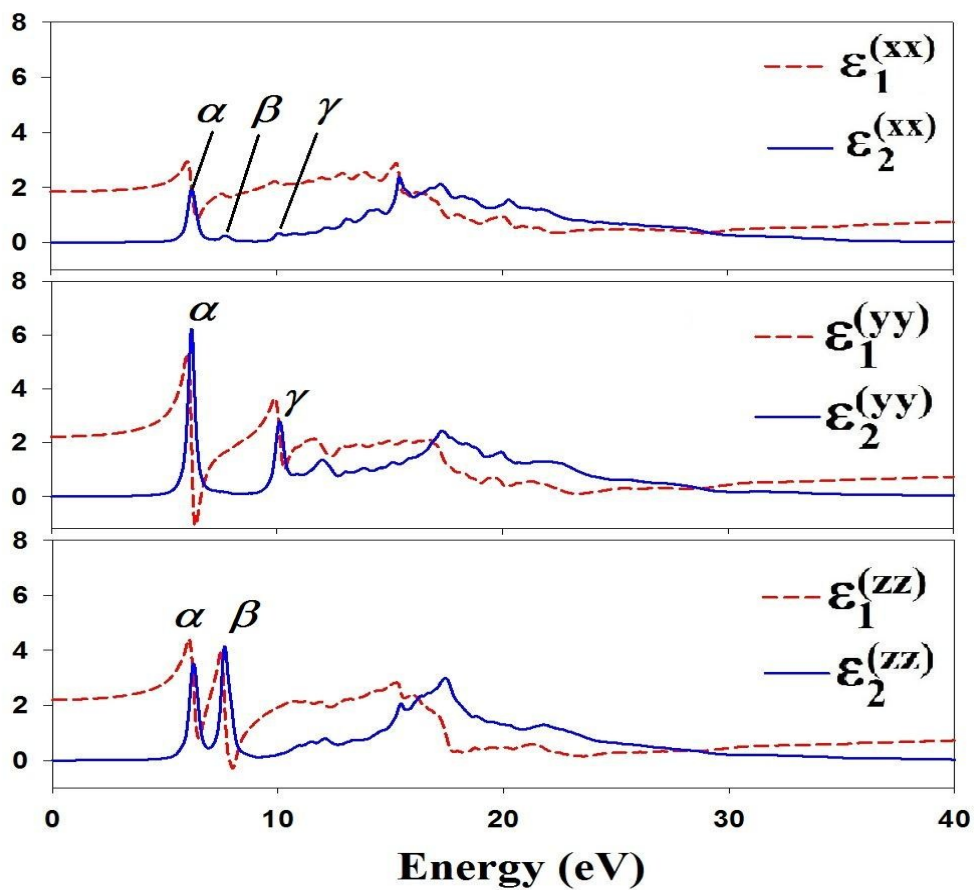


Fig. 4. Calculated imaginary (ϵ_2^{ii}) and real parts (ϵ_1^{ii}) of dielectric function for GSN crystal using mBJ approximation.

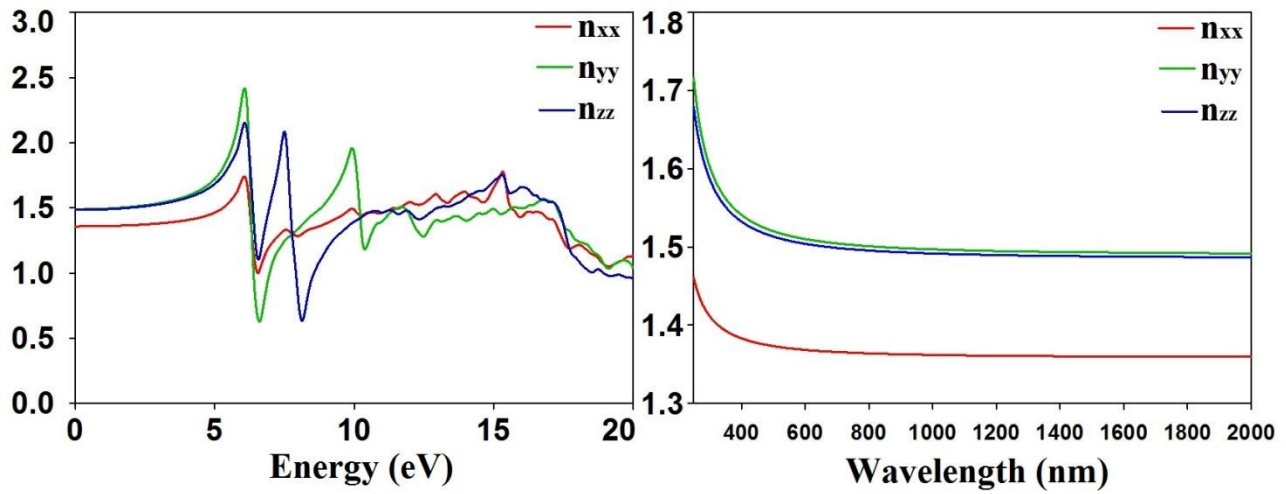


Fig. 5. Theoretical results for the refractive indices of GSN crystal.

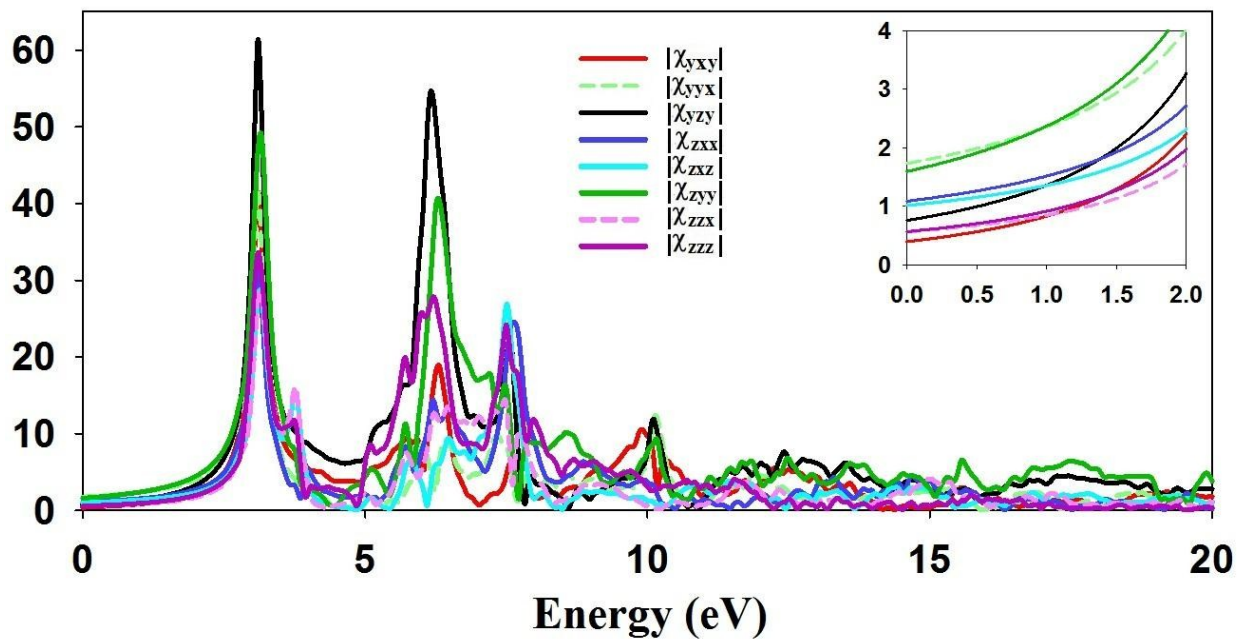


Fig. 6. Absolute values of $\chi_{ijk}^{(2)}$, in units of (pm/V), for GSN crystal.

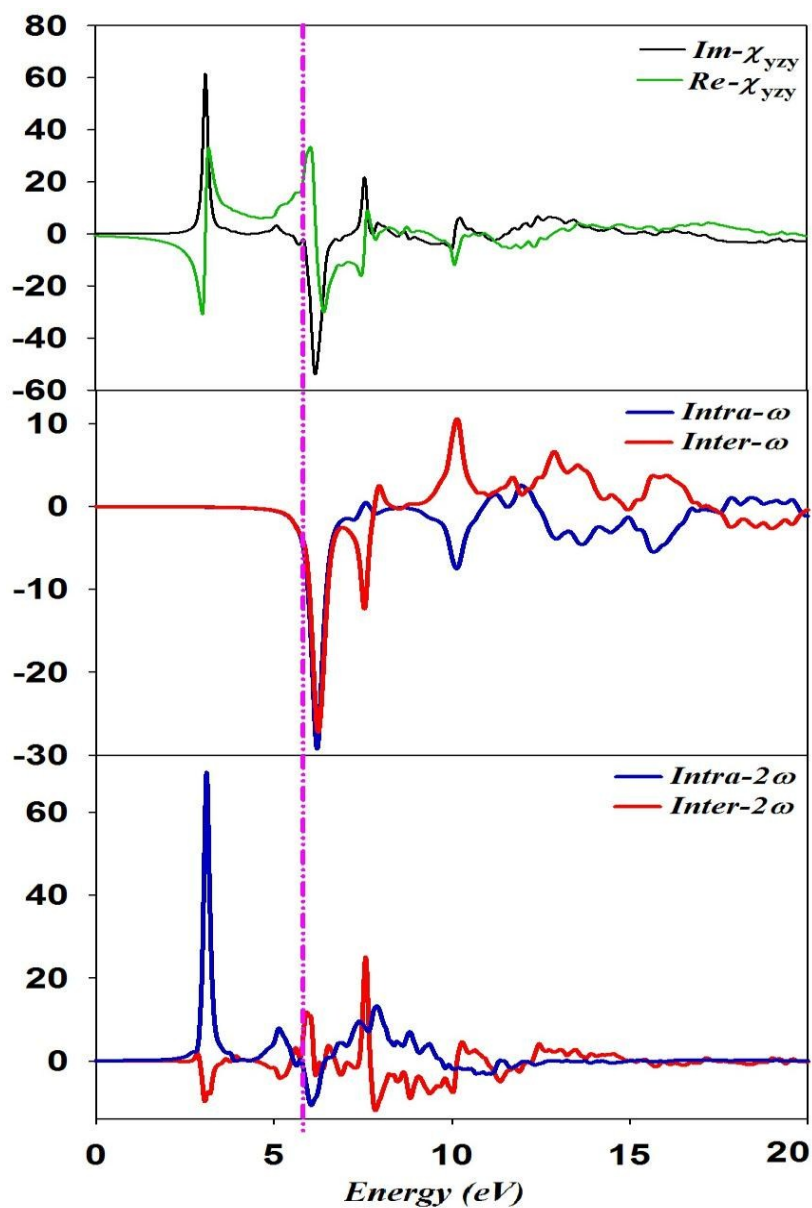


Fig. 7. The imaginary and real parts of $\chi_{zy}^{(2)}$ as well as $\omega/2\omega$ intra- and inter-band contributions to it in units of (pm/V).

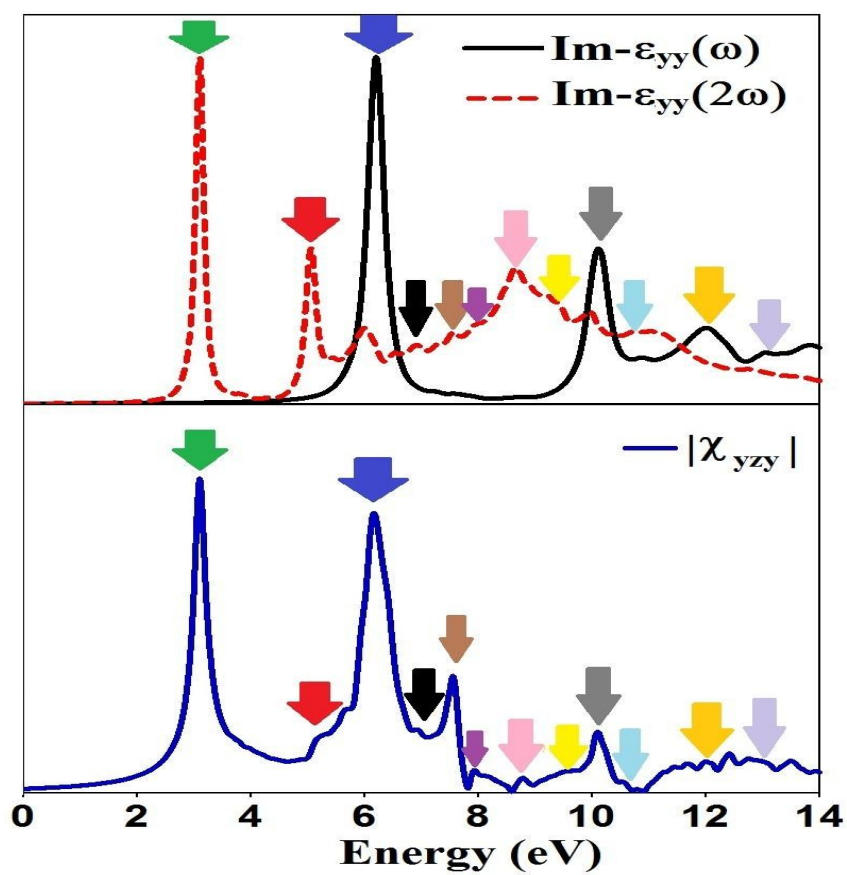


Fig. 8. Linear optical response in comparison with nonlinear one for GSN crystal.

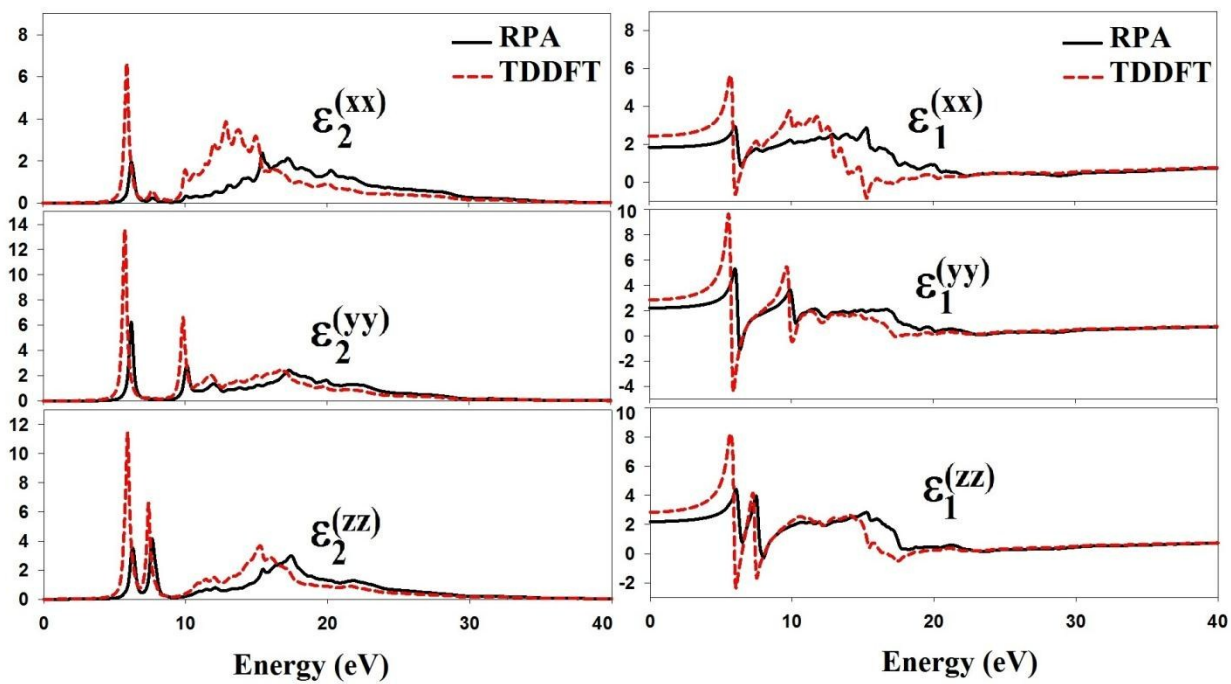


Fig. 9. The RPA and TDDFT results for the imaginary ($\epsilon_2^{(ii)}$) and real ($\epsilon_1^{(ii)}$) parts of dielectric function of GSN crystal.

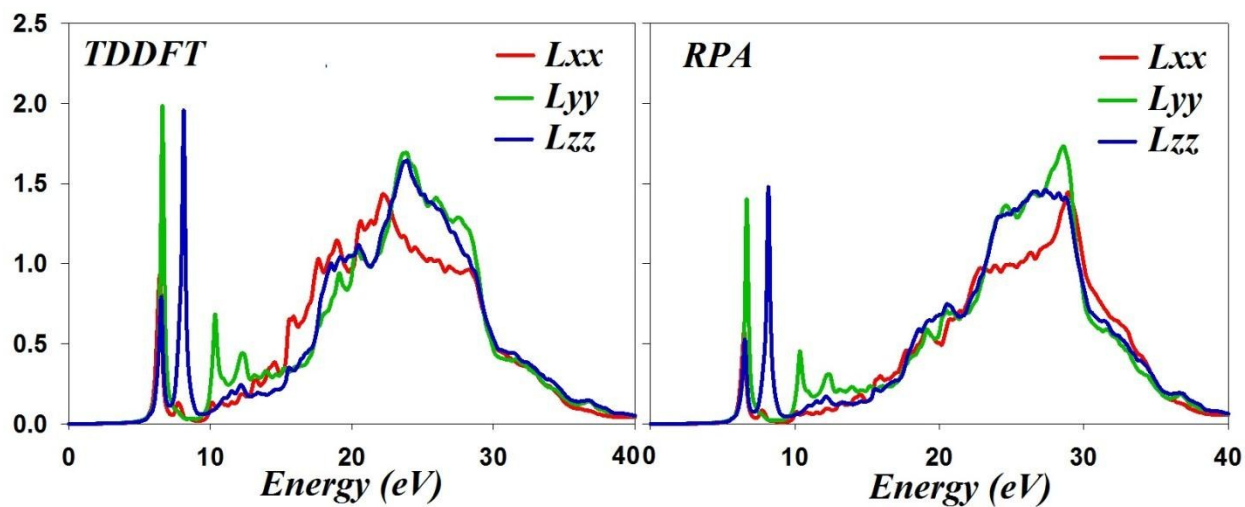


Fig. 10. The RPA and TDDFT results for the energy loss spectra of GSN crystal.

Table1: Optimized values of GSN crystal using FHI-aims code.

Bond angle	Optimized values (°)	Experimental* data (°)	Bond length	Optimized values (Å)	Experimental* data (Å)
O2-N1-O4	119.592	119.066	N1-O2	1.2700	1.2410
O2-N1-O3	119.742	120.464	N1-O3	1.2632	1.2350
O3-N1-O4	120.664	120.467	N1-O4	1.2647	1.2465
Na5-O6-C7	126.746	130.951	Na5-O6	2.4457	2.4099
O6-C7-O8	126.106	126.025	O6-C7	1.2692	1.2419
O8-C7-C9	115.954	116.186	C7-O8	1.2670	1.2472
O6-C7-C9	117.928	117.759	C7-C9	1.5241	1.5199
C7-C9-H11	108.863	109.209	C9-H10	1.0951	0.9696
C7-C9-N12	112.730	111.924	C9-H11	1.098	0.9701
C7-C9-H10	110.005	109.250	C9-N12	1.4845	1.4802
H10-C9-H11	107.150	107.967	N12-H13	1.0599	0.8899
H10-C9-N12	109.340	109.224	N12-H14	1.0509	0.8896
H11-C9-N12	108.586	109.183	N12-H15	1.0313	0.8898
C9-N12-H13	109.702	109.493	Na5-O4	2.6324	2.6146
C9-N12-H14	111.476	109.482	Na5-O2	2.5710	2.6473
C9-N12-H15	109.364	109.547			
H13-N12-H14	110.633	109.461			
H13-N12-H15	107.167	109.414			
H14-N12-H15	108.386	109.430			

Refs*. [46,47]

